Final Draft
of the original manuscript:

Lozano, G.A.; Na Ranong, C.; Bellosta von Colbe, J.M.; Bormann, R.; Fieg, G.; Hapke, J.; Dornheim, M.**:**

Empirical kinetic model of sodium alanate reacting system (II). Hydrogen absorption

In: International Journal of Hydrogen Energy (2010) Elsevier

DOI: 10.1016/j.ijhydene.2010.04.142

Empirical kinetic model of sodium alanate reacting system (II). Hydrogen desorption

Gustavo A. Lozano[a,*], Chakkrit Na Ranong[b], Jose M. Bellosta von Colbe[a], Rüdiger Bormann[a], Georg Fieg[b], Jobst Hapke[b], Martin Dornheim[a]

[a] Institute of Materials Research, GKSS Research Centre Geesthacht, D-21502 Geesthacht, Germany

[b] Institute of Process and Plant Engineering, Hamburg University of Technology, D-21073 Hamburg, Germany

Abstract

Simulation and design of hydrogen storage systems based on metal hydrides require appropriate quantitative kinetic description. This paper presents an empirical kinetic model for the two-step hydrogen desorption of sodium alanate material doped with aluminium-reduced $TiCl_4$, produced in kg-scale. The model is based on kinetic data obtained by volumetric titration measurements within a range of experimental conditions varying from 0 bar to 35 bar and from 100 °C to 190 °C. It is shown that while the first desorption step is a zero-order reaction, the second desorption step follows the Johnson-Mehl-Avrami (JMA) equation with $n = 1$. The predictions of the model are validated by experimental results and are used to asses the pressure-temperature (p-T) performance of the desorption steps against selected hydrogen supply criteria. This paper complements a previous paper of this investigation that presented the kinetic model of the corresponding hydrogen absorption of sodium alanate material.

1. Introduction

* Corresponding author Tel.: +49 41 5287 2643; fax: +49 41 5287 2625. Email address: gustavo.lozano@gkss.de (Gustavo A. Lozano)

Nowadays, many efforts are devoted to implement hydrogen as energy carrier in a clean-energy concept in mobile applications. The hydrogen storage system, which has to be oriented to certain defined parameters and restrictions such as hydrogen storage capacity and hydrogen delivery rate [1], is one of the central challenges. Simulation, design and evaluation of hydrogen storage systems that are based on metal hydrides require appropriate kinetic equations [2-5], e.g. to predict p-T conditions that allow for a desired hydrogen supply rate. This paper proposes an empirical kinetic model for the hydrogen desorption of sodium alanate material doped with aluminium-reduced $TiCl_4$, produced by a technologically applicable process in kg-scale. This is the second paper of a two-part investigation. The first part presented the kinetic model of the corresponding hydrogen absorption of sodium alanate material [6].

Bogdanovic and Schwickardi [7] showed that hydrogen can be reversibly stored in and released from sodium alanate if doped with titanium compounds. $NaAlH_4$ is reversibly formed in a two-step reaction within the technically favourable range of up to 125 °C, as shown in Eqs.1 and 2. It has a theoretical gravimetric hydrogen storage capacity of 5.6 wt% based on the absorbed material, or 5.9 wt% if based on the desorbed material.

$$3NaH + Al + 1.5H_2 \leftrightarrow Na_3AlH_6 \quad (\Delta H_R = -47\ \text{kJ mol}\ H_2^{-1}) \tag{1}$$

$$Na_3AlH_6 + 2Al + 3H_2 \leftrightarrow 3NaAlH_4 \quad (\Delta H_R = -37\ \text{kJ mol}\ H_2^{-1}) \tag{2}$$

Previous experimental investigations determined kinetic expressions for the desorption steps of sodium alanate doped with $TiCl_3$ [8, 9], Ti_{13}·6THF [10], $Ti(OBu^n)_4$ and $Zr(OBu^n)_4$ [11]. They mainly focused on the determination of the energy of activation of the Arrhenius equation. However, the hydrogen back-pressure in the desorptions and its effect on the kinetics are not reported in most of these investigations [8, 10, 11]. Luo and Gross [9] studied the effect of hydrogen back-pressure up to 3 bar, Bellosta von Colbe et al. went up to 3.75 bar [12]. The present investigation proposes an empirical kinetic model supported on experimental desorptions carried out at temperatures from 100 °C to 190 °C under hydrogen back-pressures from 0 bar up to 35 bar. This interval includes conditions which appear in the operation of practical applications and at which so far no previous measurements were reported. The utilized approach allows the independent study of each desorption step of sodium alanate material. The obtained empirical kinetic equations consider the effect of the

temperature and hydrogen back-pressure as well as the transformed fraction of the material. The investigation is complemented by the mathematical model for the evaluation of the two desorption steps as two consecutive reactions. A new approach for the material balance of the desorption steps is presented.

2. Kinetic equations

In an analogous way as the previous investigation on hydrogen absorption [6], the kinetic equations of the model are presented for the case of hydrogen desorption. The model consists of two consecutive desorption steps, and only their net rate of reaction is considered. Equations 3 and 4 define the stoichiometry of the first and second desorption steps, respectively. Equation 4 includes the additional aluminium and hydrogen produced in the first desorption step.

$$3NaAlH_4 \rightarrow Na_3AlH_6 + 2Al + 3H_2 \quad (3)$$

$$Na_3AlH_6 + 2Al + 3H_2 \rightarrow 3NaH + 3Al + 4.5H_2 \quad (4)$$

Three mixtures of defined composition are used to describe the reacting system:

$$S_I = 3NaH + 3Al + 4.5H_2 \quad (5)$$

$$S_{II} = Na_3AlH_6 + 2Al + 3H_2 \quad (6)$$

$$S_{III} = 3NaAlH_4 \quad (7)$$

Thus, Eqs. 3 and 4 correspond to Eqs. 8 and 9, respectively:

$$S_{III} \rightarrow S_{II} \quad (8)$$

$$S_{II} \rightarrow S_I \quad (9)$$

The transformed fraction α is used to follow the progress of the desorption steps and is individually considered for each desorption step. It corresponds to the ratio of mass of hydrogen that has been desorbed, m_{H_2}, to the maximal mass of hydrogen that could be desorbed, $m_{H_2,\max}$, Eq. 10. Equations 11 and 12 present an equivalent definition for each desorption step in terms of the masses of the mixtures of defined composition.

$$\alpha = \frac{m_{H_2}}{m_{H_2,\max}} \tag{10}$$

$$\alpha_{S_{III} \to S_{II}} = \frac{m_{S_{II}}}{m_{S_{III}} + m_{S_{II}}} \tag{11}$$

$$\alpha_{S_{II} \to S_{I}} = \frac{m_{S_{I}}}{m_{S_{II}} + m_{S_{I}}} \tag{12}$$

The net rate of reaction of each desorption step is defined in terms of the transformed fraction:

$$\frac{d\alpha}{dt} = k(T, p)g(\alpha) \tag{13}$$

The underlying kinetic processes of the desorption, and specially the rate-limiting process, determine the net rate of reaction and consequently the function $g(\alpha)$. The function $g(\alpha)$ is empirically determined by comparing the transformed fraction during the experiments with the value predicted by the integrated equation of different kinetic models, see Table 1 in [6]. The model equation with best-fit results defines the most appropriate function $g(\alpha)$. The evaluated kinetic equations for the description of the sorption reaction and solid phase transformation correspond to the surface controlled model, the JMA equation (nucleation and growth of the new phase begins randomly in the bulk and at the surface) and the contracting volume model (nucleation starts at the surface of the particle and growth continues from the surface into the bulk). Rudman [13] and Barkhordarian et al. [14] discuss in detail the applied models and the phenomenology behind them.

The empirical rate constant k in Eq. 13 is a function of the temperature and the hydrogen back-pressure:

$$k(T, p) = \left(Ae^{-\frac{E_a}{RT}} \right) f\left(p, p_{eq}\right) \tag{14}$$

The first factor in Eq. 14 is the Arrhenius formula, while the second factor reflects the influence of the equilibrium pressure and the hydrogen back-pressure on the net rate of reaction. This influence is a consequence of the reversible character of the reaction. The factor $f(p, p_{eq})$ acts as the driving force of the absorption, which depends on the deviation of p from p_{eq}. In this work, the factor $f(p, p_{eq})$

is defined by trying different functions and selecting the one that best fits the experimental data. Some of the considered functions are $\ln(p_{eq}/p)$ (since it defines the change of free energy of the sorption process), $(p_{eq}-p)/p_{eq}$ (a first order approximation of the logarithm based on its Taylor series), and combinations of them. However, other empirical functions may be also tried for the factor $f(p, p_{eq})$.

3. Experimental procedures

The method of material preparation and the utilized apparatus for the kinetic measurements are explained elsewhere [6, 15, 16]. The apparatus and the geometry of the cell were selected to assure in good approximation isothermal and isobaric conditions during the experiments.

The reaction kinetics of each desorption step was individually investigated by choosing specific p-T pairs for the initial and final states. At time 0 of the experiment the initial hydrogen back-pressure is stepwise changed to the hydrogen back-pressure of the final state, while the temperature remained constant. The thermodynamically stable states of the reacting system according to p-T conditions are presented in Fig. 1. The equilibrium lines are calculated using the van 't Hoff equation and the parameters determined in [17] for the sodium alanate reacting system. Equations 15 and 16 are the van 't Hoff equilibrium lines for the first and second desorption steps, respectively.

$$\ln\left(\frac{p_{eq,S_{II}\leftrightarrow S_{III}}}{1\,\text{bar}}\right)=\frac{\Delta H_{R,S_{II}\leftrightarrow S_{III}}}{RT}-\frac{\Delta S_{R,S_{II}\leftrightarrow S_{III}}}{R}=-\frac{37\,\text{kJ mol H}_2^{-1}}{R\cdot T}+\frac{122\,\text{J mol H}_2^{-1}\,\text{K}^{-1}}{R} \quad (15)$$

$$\ln\left(\frac{p_{eq,S_{I}\leftrightarrow S_{II}}}{1\,\text{bar}}\right)=\frac{\Delta H_{R,S_{I}\leftrightarrow S_{II}}}{RT}-\frac{\Delta S_{R,S_{I}\leftrightarrow S_{II}}}{R}=-\frac{47\,\text{kJ mol H}_2^{-1}}{R\cdot T}+\frac{126\,\text{J mol H}_2^{-1}\,\text{K}^{-1}}{R} \quad (16)$$

Table 1 summarizes initial and final conditions used to study each desorption reaction. All the experimental results for the kinetic analysis correspond to measurements of material that had been absorbed and desorbed for at least 3 times, when the material shows reproducible kinetics with respect to cycling.

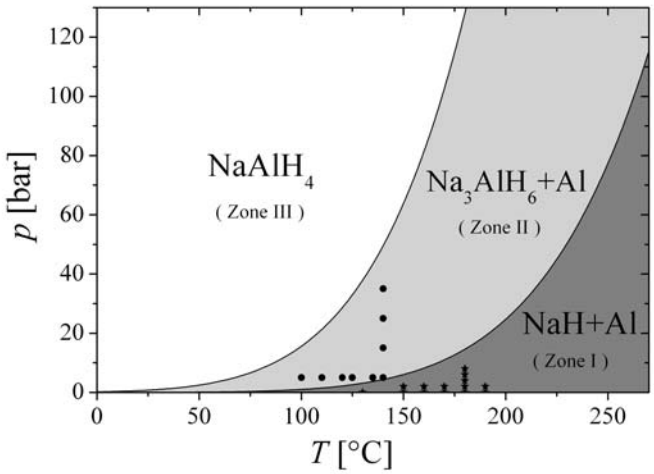

Figure 1. Stable states of the sodium alanate reacting system under hydrogen pressure at different p-T conditions. At p-T conditions inside zone I, II and III, the most stable solid states are NaH+Al, Na_3AlH_6+Al, and $NaAlH_4$, respectively. The circles (●) and the stars (★) correspond to p-T conditions for the final state of experiments for the first and second desorption steps, respectively.

Table 1. Location of the initial and final states for the desorption experiments according to the zones on Fig. 1

Desorption step	Reaction	Initial State	Final State
First	$3NaAlH_4 \rightarrow Na_3AlH_6 + 2Al + 3H_2$	Zone III	Zone II
Second	$Na_3AlH_6 + 2Al + 3H_2 \rightarrow 3NaH + 3Al + 4.5H_2$	Zone II	Zone I

4. Results and Discussion

4.1 Hydrogen desorption of $NaAlH_4$ forming Na_3AlH_6+Al: $S_{III} \rightarrow S_{II}$

Desorption experiments were carried out at different p-T conditions with starting state within zone III and final state within zone II (see Fig. 1). Previous absorptions with final conditions within zone III guaranteed the starting state of the material within this zone for the subsequent desorption. The experimental desorptions yielded hydrogen capacities of about 2.3 wt%, agreeing with the obtained

results for the second absorption step [6]. For further evaluation, the transformed fraction $\alpha_{S_{III} \rightarrow S_{II}}$ considers only the active reacting material referred to the total hydrogen desorbed in every experiment after completion and therefore goes always from 0 to 1.

Figure 2 shows hydrogen desorptions performed at 5 bar and temperatures between 100 °C and 140 °C. All desorptions start immediately and remain at constant rate without showing an incubation period or an inflection. Such a linear behaviour hints at surface reaction limited kinetics. It changes only when the transformed fraction is close to 1 and the maximal experimental capacity is almost reached. As expected because of the endothermic nature of the desorption process, the rate of desorption always increases with temperature. At 140°C and 5 bar full desorption is done in less than 5 minutes.

The desorptions at 140 °C under hydrogen back-pressures between 5 bar and 35 bar also start immediately and their slopes have the same qualitative behaviour, as shown in Figure 3. The hydrogen back-pressure shows a clear effect on the rate of desorption. For example, by reducing the hydrogen back-pressure from 25 to 5 bar, the rate of desorption approximately doubles.

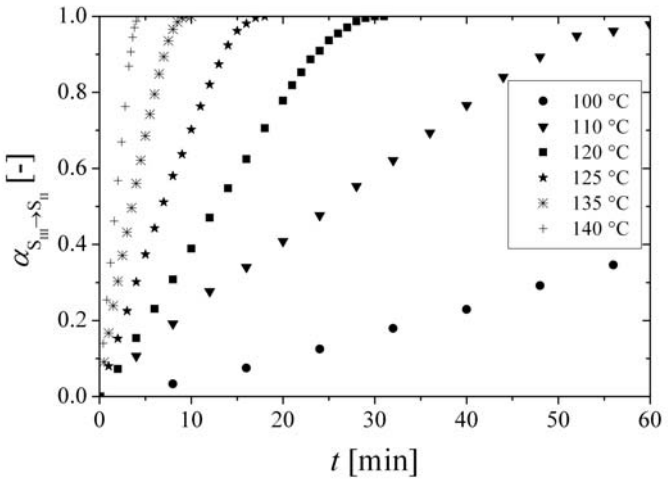

Figure 2. Desorptions of $NaAlH_4$ forming Na_3AlH_6+Al at 5 bar and temperatures between 100 °C and 140 °C. The transformed fraction is normalized to the total mass of hydrogen desorbed in each experiment after completion.

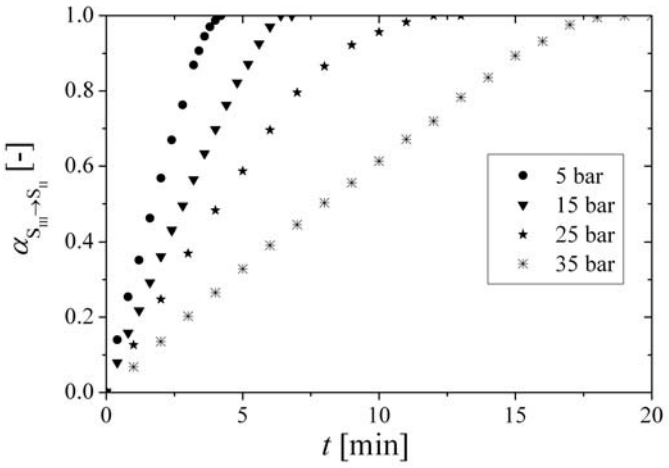

Figure 3. Desorptions of $NaAlH_4$ forming Na_3AlH_6+Al at 140 °C and hydrogen back-pressures between 5 bar and 35 bar

As mentioned before, the rate of desorption of $NaAlH_4$, when transforming to Na_3AlH_6+Al and releasing H_2, has a linear behaviour corresponding to a zero-order reaction, which is characteristic of surface controlled kinetics [14]. The best fitting for Eq. 13 is obtained the function $g(\alpha)=1$. Thus, Eq. 13 for this desorption reaction corresponds to:

$$\frac{d\alpha_{S_{III}\rightarrow S_{II}}}{dt}=k_{S_{III}\rightarrow S_{II}} \tag{17}$$

This result agrees with the results of Sandrock et al. [8], who also reports a constant rate of reaction, independent of the transformed fraction. However, it is in contrast with the first order kinetic equation reported by Luo and Gross using $TiCl_3$ [9] and Kiyobayashi et al. using $Ti(OBu^n)_4$ and $Zr(OBu^n)_4$ [11] for the desorption of $NaAlH_4$ forming Na_3AlH_6.

The fitting procedure of the constant $k_{S_{III}\rightarrow S_{II}}$, based on Eq. 14, yields as best fitting function:

$$f_{S_{III}\rightarrow S_{II}}(p,p_{eq})=\left(\left(p_{eq}-p\right)/p_{eq}\right)^2+1.04\left(\left(p_{eq}-p\right)/p_{eq}\right) \tag{18}$$

with Arrhenius parameters A=5.41×10^{10} s^{-1} and E_a=105.85 kJ mol^{-1}. Figure 4 shows the results of the fitting of the experimental data by use of these function and parameters. An increment of temperature will affect the rate of reaction not only by the Arrhenius factor but also by the function

$f_{S_{III}\rightarrow S_{II}}(p, p_{eq})$ through the equilibrium pressure $p_{eq}(T)$. By increasing the temperature, the value p_{eq} increases and thus the difference $p_{eq} - p$. This makes the driving force represented by $f_{S_{III}\rightarrow S_{II}}(p, p_{eq})$ larger and consequently the rate of reaction increases.

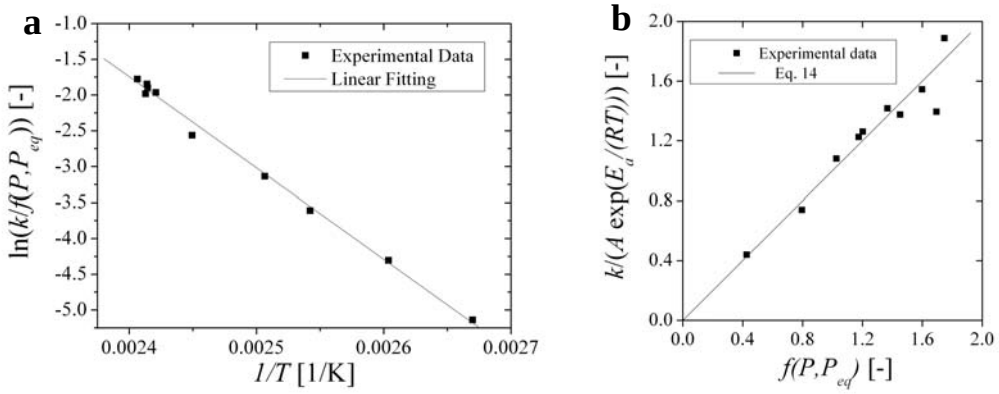

Figure 4. Kinetic fitting of the desorption of $NaAlH_4$ forming Na_3AlH_6+Al. Equation 14 defines the fitting relation. The parameters A and E_a in the right diagram (b) come from the fitting in the left diagram (a) (A=5.41×10^{10} s^{-1} and E_a =105.85 kJ mol^{-1}).

The rate constant $k_{S_{III}\rightarrow S_{II}}$ is calculated for several conditions p-T by using the functions and parameters determined through the fitting and then plotted in Fig. 5. When the hydrogen back-pressure is higher than the equilibrium pressure of the first desorption step, the rate constant is 0 by definition. By increasing the temperature as well as by decreasing the hydrogen back-pressure the value of the rate constant increases, the effect of the temperature being higher than the effect of the hydrogen back-pressure. The constant rate lines of the contour also demonstrate that by changing conditions it is possible to have the same rate of reaction at different temperatures by modifying the hydrogen back-pressure e.g. the desorption at 140 °C and 20 bar and at 130 °C and 0 bar.

The minimum value of $k_{S_{III}\rightarrow S_{II}}$ was calculated using Eq. 17 and plotted also in Fig. 5 (dashed line), such that the material during the first desorption step fulfils the discharging rate (max) of hydrogen in a fuel cell vehicle. The calculation assumed the conditions defined in [1]: hydrogen discharging rate of 2 g s^{-1} and a total storage mass of 6 kg of hydrogen. This minimum value of $k_{S_{III}\rightarrow S_{II}}$ corresponds to

0.034 min^{-1}. Under this condition, temperatures starting from 120 °C can maintain 6 bar of hydrogen back-pressure. Temperatures lower than 114 °C are not sufficient at any level of hydrogen back-pressure to fulfil the required discharging rate. This analysis is necessary in the evaluation and design of hydrogen storage systems based on metal hydrides; for example, when determining p-T working conditions if wishing to integrate the waste heat from a fuel cell with the heating system for the desorption of hydrogen from the hydride in a fuel cell powered system.

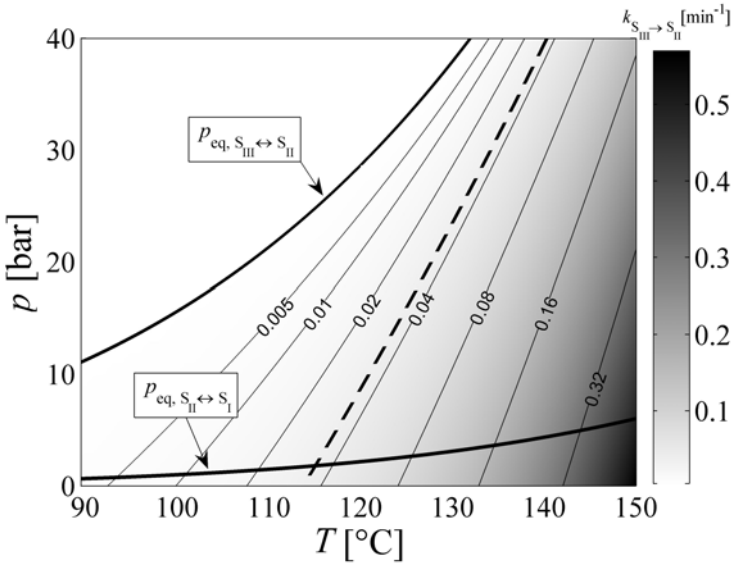

Figure 5. Calculated values of the rate constant $k_{S_{III}\rightarrow S_{II}}$ as a function of temperature and hydrogen back-pressure. The contour lines represent points with the same value of rate constant. The dashed line (---) is the minimum value of $k_{S_{III}\rightarrow S_{II}}$ that fulfils the discharging rate conditions defined in [1]

4.2 Hydrogen desorption of Na_3AlH_6 forming NaH+Al: $S_{II} \rightarrow S_I$

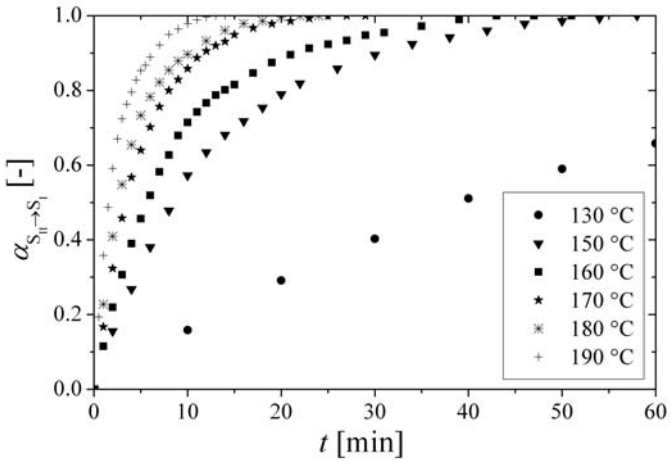

Figure 6. Desorptions of Na_3AlH_6 at 0 bar and different temperatures.

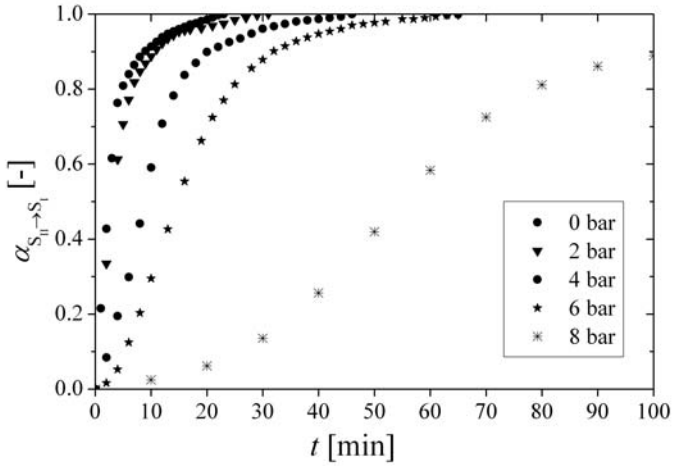

Figure 7. Desorptions of Na_3AlH_6 at 180 °C and different hydrogen back-pressures.

The desorptions of Na_3AlH_6, $S_{II} \rightarrow S_I$, had a starting state inside zone II and final state inside zone I. Previous absorptions under conditions inside zone II ensured the starting state in this zone for these desorptions. The experimental capacities measured for this desorption step were around 1.6 wt%, in agreement with the measured capacities during the absorption experiments for this step [6]. Figure 6 shows the results of the hydrogen desorptions at different temperatures under a hydrogen back-pressure of 0 bar (ca. 50 mbar). The rate of desorption increases with the temperature, at 190 °C requiring 10 min to desorb more than 97% of the hydrogen stored. The desorptions start immediately,

and in contrast to the case of $NaAlH_4$, desorption of Na_3AlH_6 forming NaH+Al does not present a linear behaviour. The rate of reaction does not stay constant as the desorption proceeds. The fitting procedure gave the JMA equation with n=1 as best representing model, Eq. 19, which is equivalent to the expression for a rate of reaction of first order:

$$\frac{d\alpha_{S_{II}\rightarrow S_I}}{dt} = k_{S_{II}\rightarrow S_I}\left(1-\alpha_{S_{II}\rightarrow S_I}\right) \tag{19}$$

An equivalent first order kinetic equation is also reported by Luo and Gross [9] and Kiyobayashi et al. [11]. However, it is in contrast to the constant rate of reaction reported by Sandrock et al. [8].

The effect of the hydrogen back-pressure on the desorption of Na_3AlH_6 is depicted in Fig. 7. During desorption the rate of reaction does not always follow a first order behaviour as the hydrogen back-pressure gets close to the corresponding equilibrium pressure. It is found that only desorption measurements performed at relatively low hydrogen back-pressures have rates of reaction of first order. At hydrogen back-pressures which draw near to the equilibrium pressure, the best fitting n parameter of the JMA equation for each measurement increases from 1 to 2, indicating a possible change in the reaction mechanism or in the rate limiting step (e.g. potential nucleation problems). Figure 8 illustrates this effect by comparing the relation between the expression $\left(p_{eq}-p\right)/p_{eq}$ and the best fitted n parameter of the JMA equation for different experiments. Under conditions far away from equilibrium $\left(p_{eq} >> p\right)$, n is close to 1. While approaching equilibrium conditions, the parameter n increases. This indicates that the model with the JMA equation n=1 is only valid if $\left(p_{eq}-p\right)/p_{eq}$>0.7.

The kinetic constant $k_{S_{II}\rightarrow S_I}$ was fitted by using $g(\alpha)=(1-\alpha)$ for all the measurements. The fitting data is best adjusted by using the function:

$$f_{S_{II}\rightarrow S_I}(p,p_{eq}) = \left(\left(p_{eq}-p\right)/p_{eq}\right)^2 - 0.46\left(\left(p_{eq}-p\right)/p_{eq}\right) \tag{20}$$

The fitted Arrhenius parameters for Eq. 14 are A=3.41×10^8 s^{-1} and E_a=91.5 kJ mol^{-1}. Figure 9 shows the comparison of the experimental data and the calculated desorption based on the model and fitted parameters. It validates the fitting for low hydrogen back-pressure with good agreement. For

desorptions at hydrogen back-pressures close to the equilibrium, the fitting deviates from the experimental data at the initial stages of reaction, see e.g. desorption at 180 °C and 6 bar in Fig. 9.

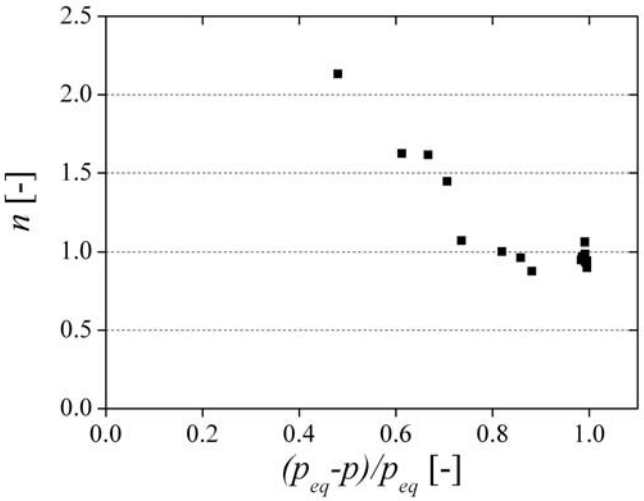

Figure 8. Best fitted JMA parameter *n* plotted against $(p_{eq} - p)/p_{eq}$ for the experimental desorption of Na_3AlH_6 at different p-T conditions.

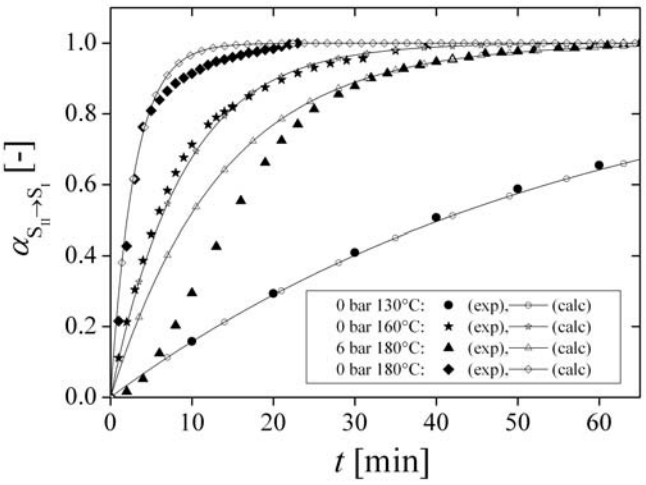

Figure 9. Experimental and calculated desorptions of Na_3AlH_6 at different p-T conditions.

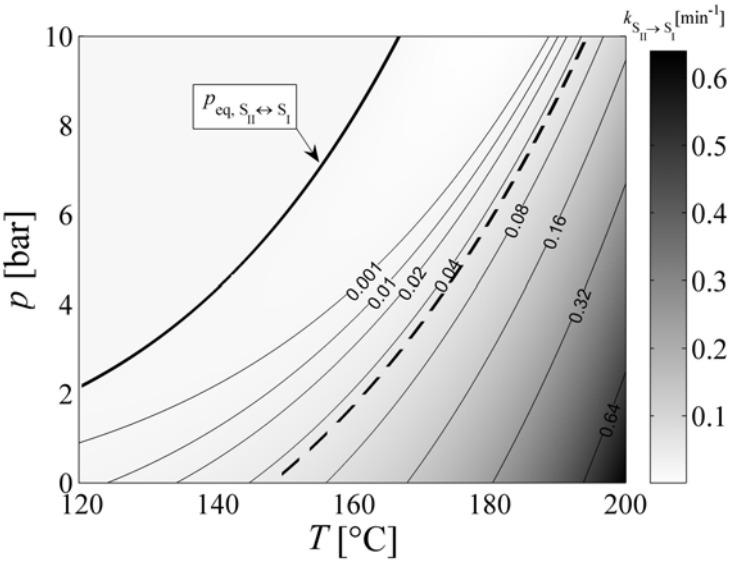

Figure 10. Calculated values of the rate constant $k_{S_{II}\rightarrow S_I}$ as a function of temperature and hydrogen back-pressure. The contour lines represent p-T conditions with the same value of rate constant. The dashed line (---) is the minimum value of $k_{S_{II}\rightarrow S_I}$ that fulfils the discharging rate conditions defined in [1] (for totally absorbed material when $\alpha_{S_{II}\rightarrow S_I}$ =0).

The calculated values of the rate constant $k_{S_{II}\rightarrow S_I}$ are shown on Fig. 10 (as similarly done in Section 4.1 for the first desorption step). At p-T conditions when the hydrogen back-pressure is higher than the equilibrium pressure of the second desorption step, the rate constant takes a value of 0 by definition. The qualitative behaviour of the rate constant of the first desorption step also applies for the rate constant of the second one in regard to temperature and pressure. By both increasing the temperature and decreasing the hydrogen back-pressure the value of the rate constant increases. Again the effect of varying the temperature is higher than the corresponding effect of the hydrogen back-pressure. Quantitatively, if compared under the same p-T conditions and by making use of Eq. 15 and the fitted parameters, the first desorption step is substantially faster than the second one. For example, at 140°C and 0 bar (ca. 50 mbar), the calculated initial hydrogen desorption rate of the first step is 10 times higher than the rate of the second desorption step. The second desorption step requires higher temperatures in order to obtain the discharging rate of hydrogen in a fuel cell vehicle [1]. At the beginning of the desorption step ($\alpha_{S_{II}\rightarrow S_I}$ =0), the temperature must be at least 147 °C to obtain the

discharging rate of 2 g s^{-1} when the hydrogen back-pressure is 0 bar. In case of the partially desorbed sample, e.g. $\alpha_{S_{II}\rightarrow S_I}$ = 0.5 and = 0.9, temperatures of 159 °C and 189 °C, respectively, are required to achieve this fast rate of desorption.

4.3 Kinetic model and validation

The desorption steps $S_{III} \rightarrow S_{II}$ and $S_{II} \rightarrow S_I$ proceed as consecutive reactions, or simultaneously. This is the case when changing conditions from zone III to I of Fig. 1. As soon as $NaAlH_4$ desorbs to Na_3AlH_6 and Al, Na_3AlH_6 desorbs further to NaH and Al because it is unstable in zone II. Desorption steps and material balances are defined in the following equations:

$$S_{III} \xrightarrow{r_{d1}} S_{II} \xrightarrow{r_{d2}} S_I \tag{21}$$

$$\frac{dm_{S_I}}{dt} = r_{d2} \tag{22}$$

$$\frac{dm_{S_{II}}}{dt} = r_{d1} - r_{d2} \tag{23}$$

$$\frac{dm_{S_{III}}}{dt} = -r_{d1} \tag{24}$$

$$r_{d1} = k_{S_{III}\rightarrow S_{II}}\left(m_{S_{III}} + m_{S_{II}}\right) \tag{25}$$

$$r_{d2} = k_{S_{II}\rightarrow S_I} m_{S_{II}} \tag{26}$$

The instantaneous rates of reaction in terms of masses, Eqs. 25 and 26, are derived from the kinetic equations of each reaction step progressing independently, Eqs. 17 and 19. A new approach for the material balance for the desorption steps is implemented, which considers that a mixture of three types of material composes the reacting system:

1. Material that can be in the three states: NaH+Al, Na_3AlH_6+Al and $NaAlH_4$.
2. Material that can be in the states NaH+Al and Na_3AlH_6+Al but not $NaAlH_4$, behaving inert for the reaction in Eq. 2
3. Material that does not react at all (inert material for both desorption steps)

The ratios of these materials are based on the hydrogen capacities experimentally measured. Table 3 in [6] shows the mass fractions of the material used in this investigation.

Calculated desorption curves based on the kinetic model are presented in Fig. 11 and experimental results are shown for comparison. It must be pointed out that the high sensitivity of the rate of reaction with respect to the experimental temperature may cause deviations from the experimentally measured, e.g. the first desorption step at 0 bar and 100 °C in Fig. 11. In general, the agreement between calculated and experimental results in terms of both the expected capacity and the kinetic behaviour is found to be very good.

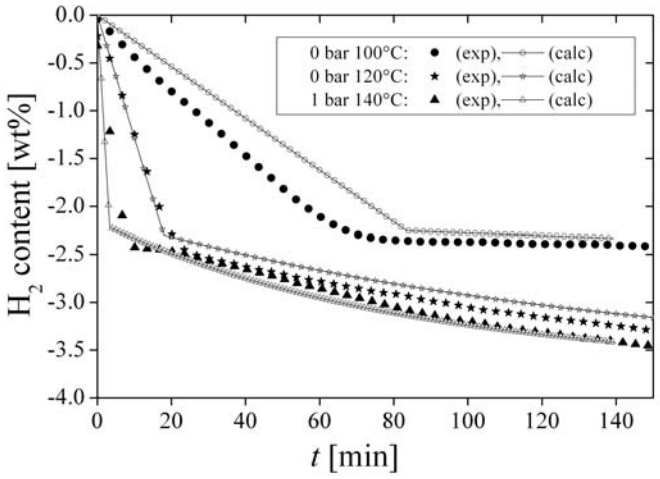

Figure 11. Experimental and calculated desorption curves of $NaAlH_4$ at different conditions. The calculations use the model presented in Section 4.3

5. Conclusions

An empirical kinetic model has been developed for the two-step hydrogen desorption of sodium alanate material, produced in kg-scale. The model takes into account not only the effect of the temperature, but also over a wide range the applied hydrogen back-pressure. It is based on results of desorption experiments at temperatures from 100 °C to 190 °C and hydrogen back-pressures from 0 bar up to 35 bar. This interval includes the conditions for practical applications and at which there are no previous measurements reported so far.

It was observed that the first desorption step follows linear kinetics like a surface controlled reaction, having a constant rate of reaction until the reaction is completed (zero-order reaction). If the

temperature is higher than 114 °C, the fitted model predicts that this desorption step is able to fulfil the specific hydrogen delivery rate for a fuel-cell vehicle as defined in (StorHy). For instance, at temperatures starting from 120 °C this desorption step can maintain the defined delivery-rate under hydrogen back-pressures of up to 6 bar. Depending on the additives used to improve the kinetics of sodium alanate as well as the preparation method, this reaction step results in the desorption of typically 2.3 wt% of hydrogen.

The second desorption step follows the JMA model with the order n =1. In case that p-T conditions draw near to the equilibrium, however, the order n of the JMA model changes and increases from 1 to 2, indicating a probable change in the reaction mechanism or in the rate limiting step (e.g. potential nucleation problems). Quantitatively, if compared under the same p-T conditions, the first desorption step is substantially faster than the second one. For example, at 140°C and 0 bar, the calculated initial hydrogen desorption rate of the first step is 10 times higher than the rate of the second desorption step. The second desorption step requires higher temperatures in order to fulfil the defined discharging rate for a fuel cell vehicle. At the beginning of the desorption step ($\alpha_{S_{II}\rightarrow S_I}$ =0), the temperature must be at least 147 °C to obtain the discharging rate of 2 g s^{-1} when the hydrogen back-pressure is 0 bar. If the material has already partially desorbed, it needs even higher temperatures. For instance, when $\alpha_{S_{II}\rightarrow S_I}$ = 0.5 or = 0.9, it requires at least 159 °C or 189 °C, respectively, to achieve this rate.

The mathematical model for the evaluation of the two desorption steps as two consecutive reactions was developed and validated against experimental desorptions. It includes a new approach for the material balance of the reactions, which categorises the material in three different types: active material for the two steps, material that can be in the states NaH and $NaAlH_6$ but not $NaAlH_4$, and inert material for both desorption steps. The ratios of the masses of each type of material are defined by the stoichiometry and the experimental hydrogen capacities. The presented model can be implemented for numerical simulation, design and evaluation of the discharging process of hydrogen storage systems based on sodium alanate.

Acknowledgments

The authors appreciate the financial support of the European Community in the frame of the Integrated Project “NESSHY—Novel Efficient Solid Storage for Hydrogen” (contract SES6-CT-2005-518271) and of the Helmholtz Initiative “FuncHy—Functional Materials for Mobile Hydrogen Storage”.

Nomenclature

A	pre-exponential factor of Arrhenius formula, s^{-1}
E_a	energy of activation of Arrhenius formula, J mol^{-1}
f	function of p and p_{eq} that acts as driving force for the absorption reaction, -
g	function that defines the rate of reaction, -
JMA	Johnson-Mehl-Avrami model
k	rate constant, s^{-1}
m	mass, kg
$m_{H_2,\max}$	maximal mass of hydrogen that could be desorbed, kg
n	kinetic order of the JMA equation, -
p	hydrogen back-pressure, bar
p_{eq}	equilibrium pressure, bar
p-T	pressure-temperature
r_{d1}	net rate of the first desorption step, kg s^{-1}
r_{d2}	net rate of the second absorption step, kg s^{-1}
R	gas universal constant, 8.314 J mol^{-1} K^{-1}
S_I	mixture of 3 mol NaH, 3 mol Al, and 9/2 mol H_2
S_{II}	mixture of 1 mol Na_3AlH_6, 3 mol Al, and 3 mol H_2
S_{III}	3 mol $NaAlH_4$
t	time, s
T	temperature, K

Greek

α transformed fraction, -

ΔH_R enthalpy of reaction per mol of hydrogen, J mol H_2^{-1}

ΔS_R entropy of reaction per mol of hydrogen, J mol H_2^{-1} K^{-1}

References

[1] StorHy. StorHy Final Publishable Activity Report. 2008. http://www.storhy.net/pdf/StorHy_FinalPublActivityReport_FV.pdf; [viewed 02.10.2009]

[2] Krokos CA, Nikolic D, Kikkinides ES, Georgiadis MC, Stubos AK. Modeling and optimization of multi-tubular metal hydride beds for efficient hydrogen storage. Int. J. Hydrogen Energy 2009;34:9128-9140.

[3] Mellouli S, Askri F, Dhaou H, Jemni A, Ben Nasrallah S. Numerical simulation of heat and mass transfer in metal hydride hydrogen storage tanks for fuel cell vehicles. Int. J. Hydrogen Energy 2010;35:1693-1705.

[4] Mellouli S, Dhaou H, Askri F, Jemni A, Ben Nasrallah S. Hydrogen storage in metal hydride tanks equipped with metal foam heat exchanger. Int. J. Hydrogen Energy 2009;34:9393-9401.

[5] Freni A, Cipitì F, Cacciola G. Finite element-based simulation of a metal hydride-based hydrogen storage tank. Int. J. Hydrogen Energy 2009;34:8574-8582.

[6] Lozano GA, Na Ranong C, Bellosta von Colbe JM, Bormann R, Fieg G, Hapke J, Dornheim M. Empirical kinetic model of sodium alanate reacting system (I). Hydrogen absorption. 2010;To be published.

[7] Bogdanovic B, Schwickardi M. Ti-doped alkali metal aluminium hydrides as potential novel reversible hydrogen storage materials. J. Alloys Compd. 1997;253-254:1-9.

[8] Sandrock G, Gross KJ, Thomas G. Effect of Ti-catalyst content on the reversible hydrogen storage properties of the sodium alanates. J. Alloys Compd. 2002;339:299-308.

[9] Luo W, Gross KJ. A kinetics model of hydrogen absorption and desorption in Ti-doped NaAlH4. J. Alloys Compd. 2004;385:224-231.

[10] Kircher O, Fichtner M. Kinetic studies of the decomposition of NaAlH4 doped with a Ti-based catalyst. J. Alloys Compd. 2005;404-406:339-342.

[11] Kiyobayashi T, Srinivasan SS, Sun D, Jensen CM. Kinetic Study and Determination of the Enthalpies of Activation of the Dehydrogenation of Titanium- and Zirconium-Doped NaAlH4 and Na3AlH6. J. Phys. Chem. A. 2003;107:7671-7674.

[12] Bellosta von Colbe JM, Felderhoff M, Bogdanovic B, Schuth F, Weidenthaler C. One-step direct synthesis of a Ti-doped sodium alanate hydrogen storage material. Chemical Communications 2005;37:4732-4734.

[13] Rudman PS. Hydriding and dehydriding kinetics. Journal of the Less Common Metals 1983;89:93-110.

[14] Barkhordarian G, Klassen T, Bormann R. Kinetic investigation of the effect of milling time on the hydrogen sorption reaction of magnesium catalyzed with different Nb2O5 contents. J. Alloys Compd. 2006;407:249-255.

[15] Dornheim M, Eigen N, Barkhordarian G, Klassen T, Bormann R. Tailoring Hydrogen Storage Materials Towards Application. Advanced Engineering Materials 2006;8:377-385.

[16] Eigen N, Keller C, Dornheim M, Klassen T, Bormann R. Industrial production of light metal hydrides for hydrogen storage. Scripta Mater. 2007;56:847-851.

[17] Bogdanovic B, Brand RA, Marjanovic A, Schwickardi M, Tölle J. Metal-doped sodium aluminium hydrides as potential new hydrogen storage materials. J. Alloys Compd. 2000;302:36-58.